1/f noise in anisotropic and giant magnetoresistive elements

1/*f* noise in anisotropic and giant magnetoresistive elements

R. J. M. van de Veerdonk[a] and P. J. L. Beliën[b]
Department of Applied Physics and COBRA, Eindhoven University of Technology, P.O. Box 513, 5600 MB Eindhoven, The Netherlands

K. M. Schep[c]
Faculty of Applied Physics and DIMES, Delft University of Technology, Lorentzweg 1, 2628 CJ Delft, The Netherlands

J. C. S. Kools,[d] M. C. de Nooijer, M. A. M. Gijs,[e] and R. Coehoorn
Philips Research Laboratories, Prof. Holstlaan 4, 5656 AA Eindhoven, The Netherlands

W. J. M. de Jonge
Department of Applied Physics and COBRA, Eindhoven University of Technology, P.O. Box 513, 5600 MB Eindhoven, The Netherlands

(Received 9 June 1997; accepted for publication 10 September 1997)

Microfabricated magnetoresistive elements based on either the anisotropic or the giant magnetoresistance effect were tested for their frequency dependent resistance noise behavior at room temperature in a dc magnetic field, using a dc sense current. Thermal resistance noise was the dominant noise source above about 10 kHz. At low frequencies the resistance noise was found to be dominated by a $1/f$ contribution that depends on the applied magnetic field. The $1/f$ noise is relatively low and field independent when the element is in a saturated state and contains a relatively large and field dependent excess contribution when the magnetic field is in the sensitive field range of the element. The $1/f$ noise level observed in saturation is comparable to the $1/f$ noise level found in nonmagnetic metals; the excess noise has a magnetic origin. The variation of the excess noise level with the applied dc magnetic field can be explained qualitatively using a simple model based on thermal excitations of the magnetization direction. © *1997 American Institute of Physics.* [S0021-8979(97)01424-2]

I. INTRODUCTION

Magnetoresistive elements (MREs) are being applied in magnetic recording read-heads and in sensor applications including position, velocity, acceleration, and angle detectors. Presently, these devices are based on the anisotropic magnetoresistance (AMR) effect,[1] which is the resistance change due to the rotation of the magnetization of a single magnetic layer with respect to the sense current. The relative resistance change in an applied magnetic field (the AMR-ratio $\Delta R_{\max}/R_0$, where $\Delta R_{\max}$ and R_0 are the maximum resistance change and the minimum resistance, respectively) is about 2% in magnetically soft permalloy ($Ni_{80}Fe_{20}$, for which below the notation Py is used) films, which are most commonly applied in high sensitivity sensors. Due to ongoing miniaturization there is a drive for more sensitive MREs, which are able to measure smaller magnetic fields or less flux (e.g., from a smaller bit on a magnetic information carrier). One of the options for improvement is the use of the giant magnetoresistance (GMR) effect,[2,3] which is the resistance change due to changing the relative orientation of the magnetization of at least two stacked magnetic layers. One of the most promising structures showing the GMR effect is the so-called spin-valve structure consisting of two magnetic layers (typically Py) separated by a nonmagnetic layer (typically Cu).[4] One of the magnetic layers has a fixed magnetization direction due to exchange biasing with an adjacent antiferromagnetic layer (typically $Fe_{50}Mn_{50}$), while the other magnetic layer is free to rotate in a small applied magnetic field. The relative resistance change (GMR-ratio) of such a spin-valve structure can be several times larger than the AMR effect for the individual magnetic layers, whereas in unpatterned films the switching takes place within approximately the same magnetic field range.[5]

To assess the applicability of GMR sensor elements the GMR-ratio and the switching field range are not the only relevant parameters. Equally important is the signal to noise ratio (see, e.g., Ref. 6). One contribution to the sensor noise is thermal resistance noise (also called Johnson or Nyquist noise), which is always present in resistive devices and is caused by thermal smearing of the distribution function of electrons near the Fermi-level. This noise source contributes a constant background to the voltage spectral density in the frequency range considered equal to $S_V = 4kTR$ (in units of V^2/Hz), where k is the Boltzmann constant, T is the temperature, and R is the total resistance of the sensor.

A second noise source is Barkhausen noise, which arises from sudden and irreversible domain wall motion. This noise

[a]Electronic mail: veerdonk@natlab.research.philips.com
Postal address: Philips Research Laboratories, Prof. Holstlaan 4, 5656 AA Eindhoven, The Netherlands.
[b]Present address: Philips Optical Storage–OPU, Industriezone 1000-1920, Kempische Steenweg 293, B-3500 Hasselt, Belgium.
[c]Present address: Philips Research Laboratories, Prof. Holstlaan 4, 5656 AA Eindhoven, The Netherlands.
[d]Present address: CVC Products, 3100 Laurelview Court, Fremont, CA 94538.
[e]Present address: Ecole Polytechnique Federale de Lausanne, Departement de Microtechnique, Institut de Microsystems, Ecublens, CH-1015 Lausanne, Switzerland.

 0021-8979/97/82(12)/6152/13/$10.00

source can be suppressed by stabilizing a single magnetic domain state and by promoting a coherent rotation process of the magnetization during switching. This can be achieved by providing an easy axis of magnetization perpendicular to the applied magnetic field, by using a specific sensor design (such as the ''picture frame'' geometry),[7] or by applying a small stabilizing magnetic field (externally or from the applied sense current, such as in the ''barber pole'' geometry).[8]

This article focusses on a third noise source, namely $1/f$ noise (also called flicker noise).[9–11] This contribution to the sensor noise is a potential limiting factor for applications of MREs as low frequency magnetic field sensors, or when sensors are miniaturized to allow for higher spatial resolution. Recently, a number of studies have been performed on the $1/f$ noise behavior of magnetic multilayers.[12–18] In these studies the amplitude of the $1/f$ noise was observed to be significantly enhanced with respect to nonmagnetic metals. This has been attributed to the complex domain structure in the studied magnetic multilayers. The lack of information on the micromagnetic structure prevented, however, a more detailed understanding.

We feel that single magnetic domain test structures in which the magnetization rotates coherently in an applied field are much better suited for the investigation of the relation between magnetism and $1/f$ noise. The magnetic state of these structures is well characterized and can be modified in a controlled way. This provides an additional knob that is accessable experimentally and that allows to change parameters reproducibly and continuously using a single device. This is in contrast to nonmagnetic materials where only the temperature can be varied.

In this article we present a comparative study of $1/f$ noise in AMR-based and GMR-based MREs. The investigated GMR-based MREs are exchange biased spin-valve structures, containing only a single magnetically sensitive layer. These elements are microfabricated in the ''picture frame'' geometry, which makes it possible to prepare a magnetic structure such that it is essentially in a single magnetic domain state.[19] It has been shown that the switching of the free layer occurs as a coherent magnetization rotation process, although the edges of the elements saturate in higher magnetic fields than the center.[20]

We find that also for these single domain structures there is a strong, magnetic field dependent contribution to the $1/f$ noise in the sensitive field range. The results are interpreted in terms of thermal excitations of the magnetization direction and explained qualitatively using a simple model based on a Stoner–Wohlfart description of the total energy.

II. EXPERIMENT

The MREs used in this study are deposited on nonmagnetic polycrystalline ceramic substrates (an Al–TiC mixture called ''Alsimag''). A layer of 30 nm Py is used for the AMR-based MRE. The GMR-based MRE consists of the multilayer 8 nm Py/2.8 nm Cu/6 nm Py/10 nm $Fe_{50}Mn_{50}$. Both MREs are grown on a buffer layer of 3.5 nm Ta and have a capping layer of 10 nm Ta. Deposition was performed by dc magnetron sputtering in a multitarget ultrahigh vacuum (UHV)-sputtering apparatus in a magnetic field in order to induce uniaxial magnetocrystalline anisotropy. The magnetic field H_l of ~15 kA/m is applied along the direction that after patterning is parallel to the long axis of the element (longitudinal direction). After deposition the films are microfabricated in a picture frame geometry using optical lithography and Ar ion milling[19] (see Fig. 1). In this geometry the magnetic layers form an almost closed yoke in order to essentially eliminate domain wall formation in the sensitive part (active area) of the MRE.

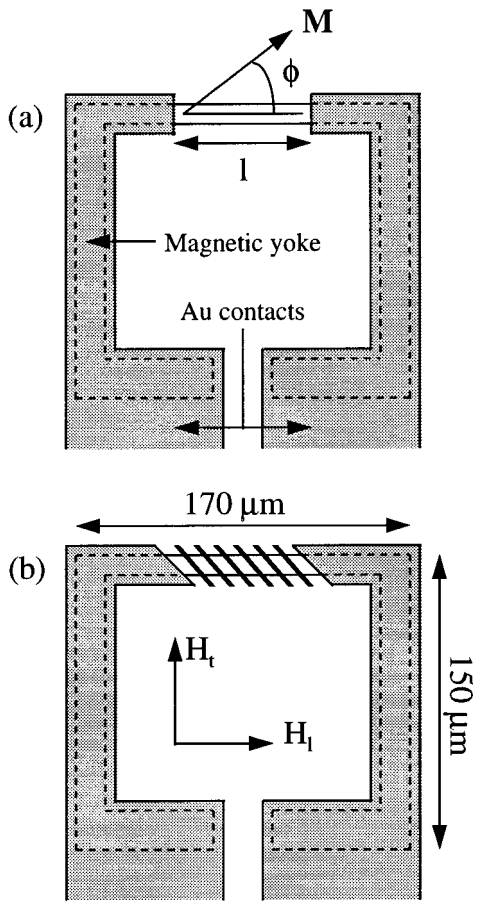

FIG. 1. Schematic representation of the geometries used for (a) the AMR-based and GMR-based MREs and (b) the AMR-based MREs with additional barber pole metallization. The 170×150 μm^2 magnetic yoke form (not shaded, also called picture frame) consists of a single magnetic layer for the AMR-based MREs and of a multilayer for the GMR-based MREs. The active area of the element is determined by the distance l between the two outermost metallization contacts (shaded). ϕ is the angle between the magnetization $\boldsymbol{M}$ and the long axis of the element. The magnetic fields H_t and H_l can be applied in the transverse and longitudinal direction with respect to the long axis of the element, respectively. The AMR-based MRE with barber pole (b) has slanted 4-μm-wide metallization stripes, spaced 7.5 μm apart (measured in the long axis direction) and at an angle of 45° with the long axis.

A 100-nm-thick gold metallization layer is used to make low resistive connections to the active area of the microfabricated (multi)layer. The active area is 10-μm-wide and varies in length l between 10 and 70 μm. The metallization layer connects on both sides to a single contact pad, which is used as both voltage and current lead. This adds a contact resistance from the metallization connections to the resistance of the active area of the MRE. The metallization connections also contribute to the noise by increasing the ther-

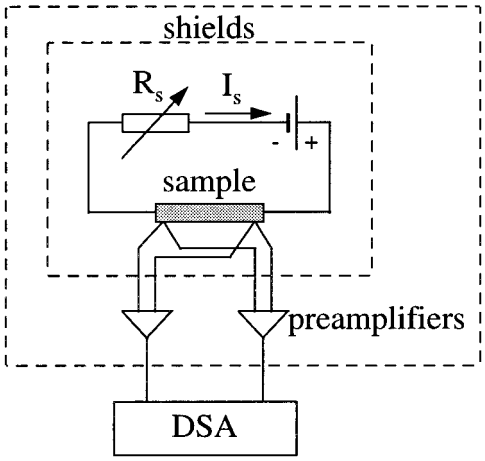

FIG. 2. Experimental setup as used for the noise measurements; all sensitive parts are placed in two mumetal shielded boxes. After preamplification, two independent signals are fed to the DSA. The Helmholtz coils (not shown) used to generate the magnetic fields are located inside the inner box.

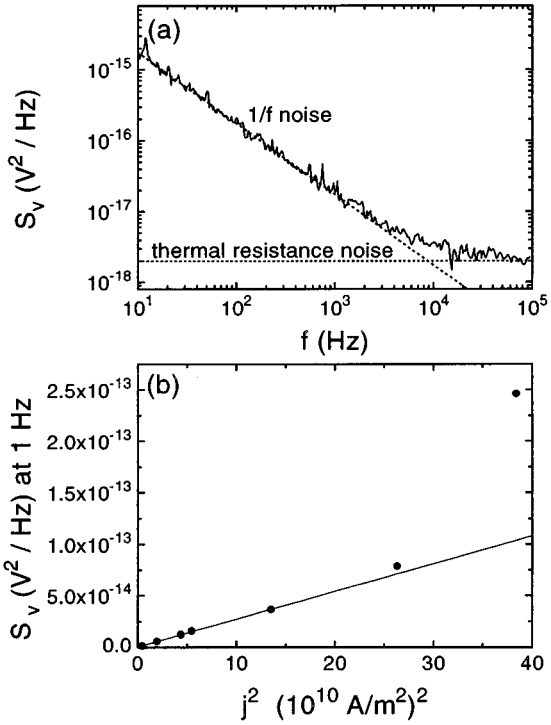

FIG. 3. (a) Example of a voltage spectral density spectrum for a GMR-based MRE with an active area length $l=70$ μm in an applied transverse magnetic field $H_t=0.50$ kA/m and for a dc sense current $I_s=2.36$ mA, corresponding to a film averaged sense current density $j=1.4\times10^{10}$ A/m^2. Thermal noise and $1/f$ noise contributions are indicated by dashed lines. (b) The voltage spectral density extrapolated to 1 Hz vs the square of the applied film averaged sense current density without applied magnetic fields follows a j^2 behavior (solid line) upto a current density $j_c\approx5\times10^{10}$ A/m^2.

mal noise and adding $1/f$ contact noise. Despite these disadvantages the two terminal geometry has been chosen over a four terminal geometry in order to resemble more closely the designs used for read-head applications. The influence of the geometry on the experimental results was verified, see below, and was found to be minor and easily distinguishable. AMR-based MREs have been fabricated both with [Fig. 1(a)] and without [Fig. 1(b)] a slanted pattern of 100-nm-thick gold stripes, a so-called barber pole metallization,[8] on top of the active part of the MRE. The barber pole metallization is commonly used to linearize the response around zero applied magnetic field and will be discussed in more detail below. The AMR-based MREs without barber pole have been microfabricated with varying length of the active area on a single substrate, which makes it possible to determine the contact resistance (noise).

After processing, the GMR-based MREs were heated to 140 °C and subsequently cooled in an applied magnetic field H_t along the short axis of the MRE (the transverse direction). This procedure rotates the exchange biasing direction of the top (or ''pinned'') magnetic layer.[19] The growth induced uniaxial magnetocrystalline anisotropy promotes hysteresis free rotation of the other (''free'') magnetic layer in an applied transverse magnetic field.[5]

The measurements have been performed in mumetal shielded boxes using the setup as shown in Fig. 2. A static magnetic field $\boldsymbol{H}=(H_l,H_t)$ can be applied in the film plane using two orthogonal sets of Helmholtz coils with a maximum field strength of about 4 kA/m each. The current for these coils is generated by mains powered supplies (Kepco BOP36-12). The sense current I_s through the MRE is provided by a battery unit and can be varied by changing the series resistor R_s. The voltage is measured by two pairs of voltage leads and is preamplified by two battery powered ultra low-noise ac voltage amplifiers with a gain of 1000 (EG&G Brookdeal 5004) before they are transferred to the analyzer. The analyzer [HP3562A dynamic signal analyzer (DSA)] was used in cross-correlation mode to minimize the spurious noise contributions of the voltage lead connections and the preamplifiers. The voltage spectral density $S_V(f,\boldsymbol{H})$ has been measured for frequencies f between 10 Hz and 100 kHz. The relative error in the presented noise levels is within $\pm10\%$.

III. EXPERIMENTAL RESULTS

An example of a spectrum for a GMR-based MRE is given in Fig. 3(a). In Fig. 3(a) the $1/f$ contribution to the spectrum is apparent in the low frequency range while at higher frequencies the noise is dominated by thermal noise (in the example the crossover frequency is ~8 kHz). The thermal noise level was never observed to deviate significantly from the expected $4kTR$ level. The results presented below will focus on the amplitude of the $1/f$ component in the spectra.

The voltage spectral density for $1/f$ noise can be described phenomenologically by the Hooge relation:[21]

$$S_V(f,\boldsymbol{H})=\frac{\alpha(\boldsymbol{H})}{Nf^{\gamma}}V_{\mathrm{dc}}^2, \tag{1}$$

where the exponent γ is of order one and the total number of conduction electrons in the sample N is taken equal to the number of atoms in the active area of the MRE. The dimensionless normalizing constant α is called the Hooge constant which for magnetic materials depends on the magnetic state which in turn depends on the applied magnetic field. The

exponent γ was also found to have a significant dependence on the applied magnetic field, which we will not discuss in this article, and ranged between 0.85 and 1.20. We will use the voltage spectral density extrapolated to 1 Hz as a measure for the $1/f$ noise. Since S_V depends on the volume and resistance of the MRE as well as the applied sense current, only α values can be used to compare the intrinsic $1/f$noise levels between different MREs. The buffer and cap layers are disregarded in the analysis of noise data because of the high resistivity of Ta.

According to the Hooge relation Eq. (1), S_V should be proportional to I_s^2 for constant applied magnetic field. In Fig. 3(b) the voltage spectral density at 1 Hz is shown to increase linearly with the square of the applied dc sense current density upto a critical film averaged current density $j_c \approx 5\times 10^{10}$ A/m^2. For higher current densities the $1/f$ noise is higher than expected from the Hooge relation Eq. (1). All experiments reported in this article have been conducted at current densities below j_c. For comparison, in our laboratory a sense current of 10 mA is the standard operating condition for all MREs. This corresponds to a current density of 6×10^{10} A/m^2) in Fig. 3(b) which is slightly above j_c.

The volume scaling predicted by the Hooge relation Eq. (1) has to be used with caution for a magnetic element due to the influence of the geometry on its magnetic properties. When the magnetic properties are changed (e.g., by varying the thickness or the width of the stripe) this will have an additional effect on the noise, mainly via the α parameter. Only the length of the active area can be varied without changing the magnetic properties. This can be done by changing the layout of the nonmagnetic metallization layer. We will use this below to estimate the contact noise contribution.

We note that for metallic thin film elements the analysis of the $1/f$ noise in terms of the Hooge relation Eq. (1) is principle incorrect due to the nonuniform current density across the film thickness. First, this is due to the effect of the film boundaries (see, e.g., Refs. 22 and 23). In multilayers an additional nonuniformity is caused by the different resistivities for the various materials and the scattering of electrons at the interfaces between them. Nevertheless, we will use Eq. (1) below as a first step towards a more complete analysis of the experimental results because we are dealing with systems for which the values of α are different by more than one order of magnitude.

A. AMR-based MRE without barber pole

The first system studied is an AMR-based MRE consisting of a 30-nm-thick Py thin film without barber pole metallization. The geometry is a narrow magnetic stripe with the sense current flowing in the longitudinal direction, see Fig. 1(a). The easy magnetization axis is along the length of the stripe and its magnetization rotates coherently in an applied transverse magnetic field H_t. The resistance is highest for the magnetization aligned parallel to the current and lowest for a perpendicular alignment. This particular geometry is well suited for initial measurements because of the high degree of symmetry both electronically and magnetically.

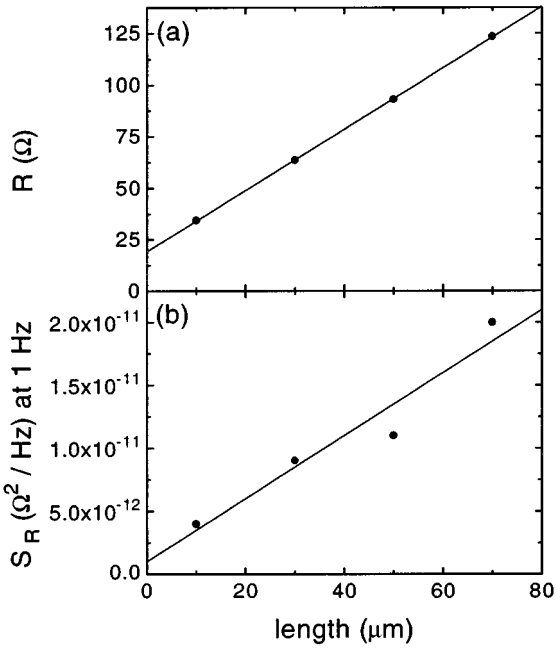

FIG. 4. Influence of the length of the active area of an AMR-based MRE without barber pole metallization on (a) the resistance and (b) the scaled $1/f$ noise level at 1 Hz without applied fields. The lines are linear fits to the data.

1. Contact resistance and contact noise

First the contact resistance and contact noise were determined from resistance and noise measurements without applied magnetic fields. In Fig. 4(a), the total MRE resistance is depicted as a function of the length of the active area. The data points extrapolate linearly towards an intercept of $19.3\pm 0.4\Omega$, which is the contact resistance. All resistance measurements reported in this article are taken from MREs with an active area length of 70 μm and have not been corrected for this nonmagnetoresistive contact resistance, although it has been taken into account in the quantitative analysis of the noise. As a result of the contact resistance, all the reported MR-ratios will be lower than their intrinsic values.

The $1/f$ contact noise contribution has been determined by measuring S_V as a function of the dc sense current using a number of similar MREs with different lengths of the active area. To compare the $1/f$ noise between these MREs the slope of the linear part of the measured voltage spectral density at 1 Hz as a function of j^2 has been used [this is the resistance spectral density at 1 Hz $S_R=\alpha R^2/N\propto l$, also see Fig. 3(b)]. In Fig. 4(b), S_R has been plotted versus the active area length. It can be fitted with a linear curve with an intercept of $(1\pm 2)\times 10^{-12}\Omega^2$/Hz due to $1/f$ contact noise. For the MREs with $l=70$ μm the $1/f$ contact noise (if any) contributes negligibly to the overall $1/f$ noise level, and has therefore, been discarded in the remainder of the article.

2. Magnetoresistance

The resistance of the MRE is shown in Fig. 5(a) as a function of an applied transverse magnetic field H_t. The smooth, hysteresis free curve indicates coherent rotation of the magnetization from the longitudinal direction in zero

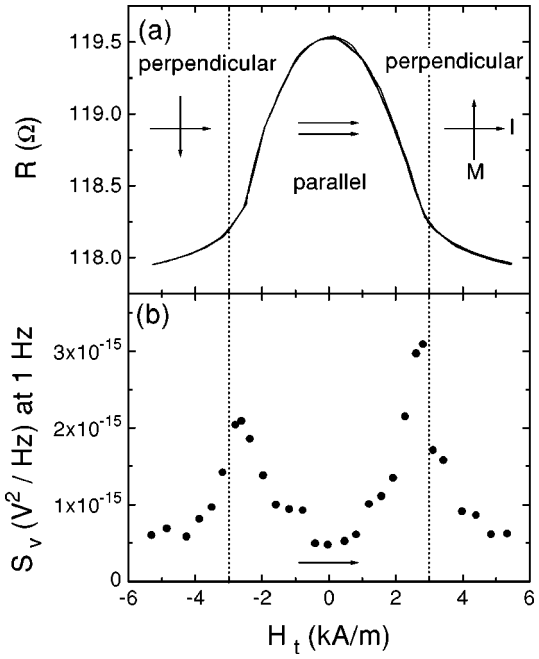

FIG. 5. Transverse magnetic field dependence of (a) the resistance and (b) the voltage spectral density at 1 Hz for an AMR-based MRE without barber pole metallization. The MR-ratio for this MRE is 1.3% in the available field range. The noise spectra have been measured with a dc sense current $I_s=5.74$ mA, corresponding to a film averaged sense current density $j=1.9\times10^{10}$ A/m^2. The dashed lines indicate the estimated saturation fields $\pm H_s$ for this geometry. The data given in (b) are taken with increasing H_t, as indicated by the arrow.

field to the transverse direction at high fields. For a uniformly rotating magnetization a parabolic behavior of the resistance versus field is expected with the saturation field H_s equal to the sum of the demagnetizing field H_d and the anisotropy field H_a. The demagnetizing field can be approximated by $H_d \approx M_s t/w = 2.6$ kA/m (M_s is the saturation magnetic moment and t/w the thickness to width ratio of the magnetic layer) and $H_a \approx 0.4$ kA/m for Py, which yields $H_s \approx 3.0$ kA/m (dashed lines in Fig. 5). For low H_t the expected parabolic behavior is observed.

The rounding of the resistance curve near H_s reflects that the edges of the stripe saturate at higher fields than the middle of the stripe. An additional rounding comes from microscopic lateral variations of the magnetization direction,[24] called ripple, which are most prominent near the saturation field.[20,25] Both the nonuniform rotation process and the ripple cause the maximum slope of the resistance curve to be reached at fields slightly below H_s. Even in the maximum available field, full saturation cannot be reached for the whole stripe in this geometry.

3. Noise

The dependence of S_V at 1 Hz on H_t is shown in Fig. 5(b); similar results have been obtained for a number of these MREs. Peaks are present at two fields close to where the maximum slope in the magnetoresistance curve is obtained. The peak values for the voltage spectral density are not equal. This is probably due to a small alignment error in the transverse magnetic field direction, which leads to an asymmetry in the measured S_V versus H_t curve. From the Hooge relation Eq. (1), values for the Hooge constant are found between $\alpha_{\min}=2.8\times10^{-3}$ and $\alpha_{\max}=1.7\times10^{-2}$ (i.e. $\sim 6\times \alpha_{\min}$). The minimum value corresponds well to values commonly found for nonmagnetic metals.[10] The observed field dependence of the excess voltage spectral density can obviously not be explained by the resistance change, via the $V_{\rm dc}^2$ term in the Hooge relation Eq. (1), as this would be a much smaller effect with a different field dependence. Thus the observed field dependence seems to clearly have a magnetic origin.

B. AMR-based MRE with barber pole

The second MRE design studied is also based on the AMR effect but its output has been linearized around zero field using the barber pole geometry.[8] On top of the active area a well conducting metallization layer is microfabricated in the form of a pattern of parallel stripes with the stripe axis rotated from the longitudinal direction [in the present case by 45°, see also Fig. 1(b)]. This effectively rotates the current direction in the magnetic layer between the metallization stripes. However, the analysis of the magnetic response is complex due to the influence of the magnetic field generated by the sense current flowing in the metallization stripes. In addition, the metallization stripes cause a nonuniform current density which complicates the analysis of the magnetoresistance and $1/f$ noise.

1. Magnetoresistance

The magnetoresistive response for this MRE to an applied transverse magnetic field H_t is shown in Fig. 6(a). The smooth, essentially hysteresis free curve again indicates a coherent rotation of the magnetization direction. A small longitudinal magnetic field $H_l=80$ A/m has in this case been applied to assure the same direction of this rotation for all applied sense currents and was sufficiently small to have negligible other effects on the measured results. As expected, the resistance varies linearly with H_t around zero field. For increasing transverse fields, a maximum or minimum in the resistance is reached when the magnetization direction is aligned along or perpendicular to the current direction in between the barber pole stripes, respectively. Increasing the transverse field further will decrease the resistance towards the zero field value for fields above the saturation field since the magnetization will again be at an angle of 45° with the current in between the barber pole stripes. The estimated saturation field is identical to H_s for the AMR-based MRE without barber pole and is indicated by dashed lines in Fig. 6). There is some rounding of the curve due to edge and ripple effects as discussed above and some asymmetry that probably arises from a small alignment error. Also in this MRE type full saturation can not be reached in the maximum available magnetic field.

2. Noise

In Fig. 6(b) the H_t dependence of S_V at 1 Hz is presented. The result is representative for a number of measured MREs. Peaks are observed close to the three magnetic fields where the slope of the magnetoresistance curve shows a local

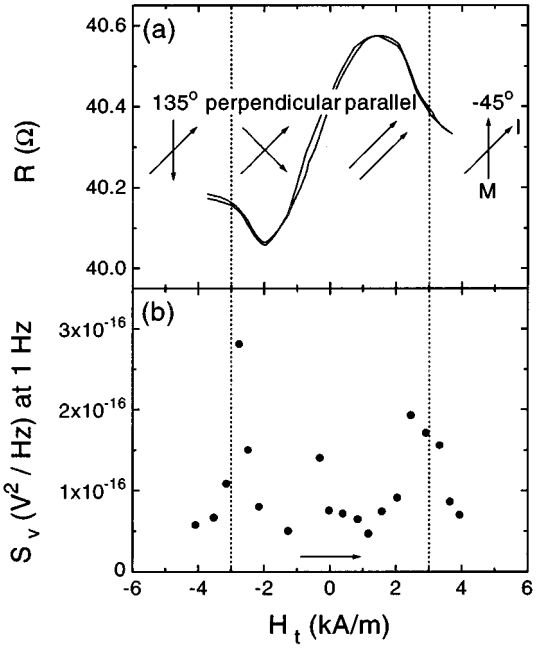

FIG. 6. Transverse magnetic field dependence of (a) the resistance and (b) the voltage spectral density at 1 Hz for an AMR-based MRE with barber pole metallization. The MR-ratio for this MRE is 1.3%. The noise spectra have been measured with a dc sense current $I_s = 2.16$ mA, corresponding to a film averaged sense current density $j = 7.2 \times 10^9$ A/m^2 (not corrected for current distribution effects due to the metallization layer) and an applied longitudinal magnetic field $H_l = 80$ A/m. The dashed lines indicate the estimated saturation fields $\pm H_s$ for this geometry. The data given in (b) are taken with increasing H_t, as indicated by the arrow.

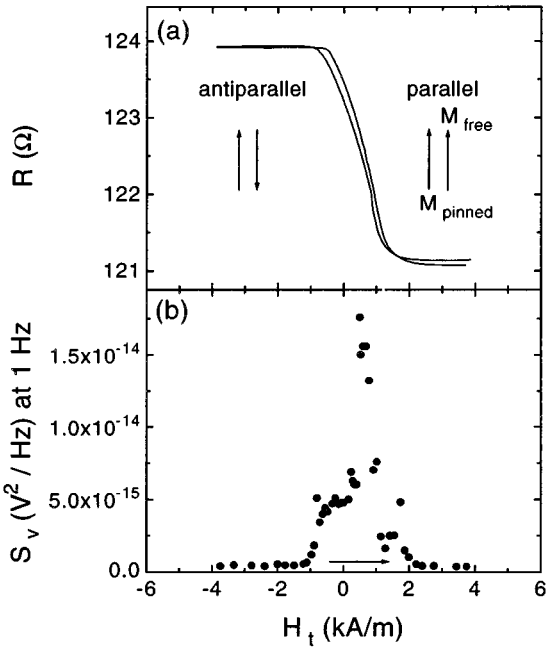

FIG. 7. Transverse magnetic field dependence of (a) the resistance and (b) the voltage spectral density at 1 Hz for a GMR-based MRE. The MR-ratio for this MRE is 2.4%. The noise spectra have been measured with a dc sense current $I_s = 2.36$ mA, corresponding to a film averaged sense current density $j = 1.4 \times 10^{10}$ A/m^2. The data given in (b) are taken with increasing H_t, as indicated by the arrow.

maximum. The α values found for this MRE vary between $\alpha_{\min} = 4.4 \times 10^{-2}$ and $\alpha_{\max} = 2.4 \times 10^{-1}$ (i.e., $\sim 5.5 \times \alpha_{\min}$), which are over an order of magnitude higher than for the AMR-based MRE without barber pole metallization. To obtain these α values, the total volume of the magnetic layer in the active area was used. Also, the same contact resistance as for the AMR-based MRE without barber pole was assumed, although the geometry of the contact metallization was different. The contact resistance and contact noise were not measured directly. As the α values depend quadratically on the resistance of the element and the assumed contact resistance is about half the total resistance, this could change the α values by at most a factor of 4. Irrespective of these uncertainties, the magnitude of the excess noise level and its field dependence point also here to a magnetic origin.

The higher α values compared to the values found for the AMR-based MRE without barber pole might be explained, at least partly, in the following way: The metallization layer reduces the effective volume of the sample by creating ''shorts'' at the places where it overlaps the magnetic layer, thus effectively reducing the volume of the magnetic layer by some (unknown) factor depending on the current distribution within the element. Therefore, the active volume is overestimated, which in turn will increase the value of α obtained from Eq. (1). Insufficient information is presently available on the current distribution and contact resistance (noise) to make a quantitative correction for these effects.

C. GMR-based MRE

The last MRE design investigated is based on the GMR effect. Use is made of an exchange biased spin-valve type element. The resistance is low when the magnetizations of the pinned and the free layer are aligned parallel and high for the antiparallel alignment. The AMR effect associated with the rotation of the free layer with respect to the current direction also contributes to the magnetoresistance.

1. Magnetoresistance

Figure 7(a) shows the magnetoresistive response to an applied transverse magnetic field H_t. The smooth curve indicates a predominantly coherent rotation process, although some hysteresis is still present. For a uniformly rotating magnetization a linear variation of the resistance with the transverse field is expected due to the GMR effect. A parabolic variation due to the AMR effect in the rotating free layer is superimposed on the GMR effect. The resistance saturates to a low (high) resistance state when the applied transverse field is increased above the saturation field and the magnetization of the free layer is aligned (anti)-parallel to that of the pinned layer. This expected behavior is indeed observed.

There is some rounding near the saturation fields, which is, however, less pronounced than in the AMR-based MREs. The estimated demagnetizing field for the free layer $H_d \approx 0.7$ kA/m is smaller than in the previously discussed MRE's due to the thinner magnetic layer. Added to the induced anisotropy field of $H_a \approx 0.4$ kA/m this leads to an estimated saturation field of $H_s \approx 1.1$ kA/m, which corresponds fairly well with the half-width of the magnetoresistance curve. We note

that a shift in the magnetic field range may occur due to the magnetic coupling between the two magnetic layers (Néel and exchange coupling across the nonmagnetic layer and magnetostatic interactions due to the stray field from the pinned layer). Combined with the parabolic distortion of the magnetoresistance curve due to the AMR effect this may shift the center of the field range of highest sensitivity away from zero field.

2. Noise

In Fig. 7(b) the corresponding H_t dependence of S_V at 1 Hz is displayed for one of the measured MREs. Similar to the results of the AMR-based MREs a large peak is observed close to the field where the maximum slope of the magnetoresistance curve is obtained, in this case at $H_t \approx 0.6$ kA/m. A shoulder is observed extending to the negative saturation field and a smaller shoulder to higher fields which is, however, not observed in all (nominally equal) MREs. From the Hooge relation Eq. (1) values for the Hooge constant between $\alpha_{\min}=6.7\times10^{-3}$ and $\alpha_{\max}=2.8\times10^{-1}$ (i.e., $\sim 42\times \alpha_{\min}$) are found, while the shoulder has $\alpha_{\text{shoulder}}=8.2\times10^{-2}$ (i.e., $\sim 12\times\alpha_{\min}$). These α values are obtained using the total volume of the multilayer and assuming the same contact resistance as for the AMR-based MRE without barber pole.

Here, $\alpha_{\min}$ is more than twice the value obtained for the AMR-based MRE without barber pole. This might be caused by a nonhomogeneous current density (on which α depends quadratically) in the direction normal to the film plane, caused by the different conductivity of Py and Cu. As a result the active volume and thereby α would be overestimated. Also the interfaces might give rise to additional $1/f$ noise. We note that the ratio between the maximum (or shoulder) and minimum noise level is much higher than for the AMR-based MREs discussed above. Again, the field dependence and the amplitude of the excess noise point to a magnetic origin.

IV. MODELLING

As has been shown above, the excess $1/f$ noise level depends strongly on the magnetic field. The origin of this excess noise may in principle be external, if it arises from noise sources in the experimental setup, as well as intrinsic. As will be shown in Sec. IV A, noise from external sources cannot explain the experimental results presented in the previous section. In Sec. IV B a model will be presented for the excess $1/f$ noise that is intrinsic to the sensor element.

A. Field fluctuations

For our experimental setup we expect that the dominant nonintrinsic source of field dependent $1/f$ noise is a fluctuating applied magnetic field, due to $1/f$ noise in the current through the Helmholtz coils. Field fluctuations give rise to resistance noise via the dependence of the resistance on the magnetic field:

$$S_R(f,H_t)=\left(\frac{\partial R}{\partial H_t'}\bigg|_{H_t'=H_t}\right)^2\times S_{H_t}(f), \tag{2}$$

where $S_R(f,H_t)$ is the resistance spectral density and $S_{H_t}(f)$ the spectral density of the applied magnetic field. The influence of the field noise is estimated from the spectral density in the current through the Helmholtz coils and is for the most noisy configuration found to be $S_{H_t}\approx 2.5\times10^{-6}$ $(\text{A/m})^2/\text{Hz}$ at 10 Hz, decreasing as $1/f$ to lower values at higher frequencies. The estimated maximum resistance noise corresponding to this level is at least one order of magnitude lower as compared to the measured $1/f$ noise levels. Also, no cross-correlation was found between the fluctuations in the resistance of the MRE and the fluctuations of the current through the Helmholtz coils. Therefore, field fluctuations may be discarded as an explanation for the observed field dependence of the resistance noise.

B. Thermal excitations

A qualitative understanding of the measured field dependence of the excess $1/f$ noise levels can be obtained from a model based on thermal excitation of the magnetic moment direction at a given nonzero temperature. The magnetic fluctuations are translated into resistance fluctuations via the dependence of the resistance on the angle of the magnetization.

In this article we calculate the effect of thermal excitations on the variances of the magnetization angle and the resistance. To obtain the variance of voltage, the variance of the resistance has to be multiplied by the dc sense current squared. These variances are equal to the frequency integrated corresponding spectral density. The frequency dependence is not calculated directly. However, it is well known that thermal excitations lead to $1/f$ noise when a sufficiently broad range of relaxation times is available around the investigated frequency range.[10] Indeed, ferromagnetic relaxation mechanisms have been measured with time constants in the μs range to the Ms range, see, e.g., Refs. 26 and 27. Since the explanation of the frequency dependence of the noise is analogous to that for nonmagnetic materials,[10] we focus completely on the magnetic field dependence of the noise which is specific for magnetic materials. To study the magnetic field dependence it is sufficient to consider the integrated noise spectrum, i.e., the variance.

In this article, we will restrict the calculations to a single magnetic layer with a uniform magnetization direction, i.e., a single magnetic domain with infinite intralayer exchange energy. The magnetic behavior of this domain is described within a Stoner–Wohlfahrt model which has been used extensively to describe the equilibrium properties of MREs, see, e.g., Ref. 28. The total magnetic energy E of the system is expressed as the sum of all relevant interaction energies and depends on the direction of the magnetization vector which is assumed to remain in the film plane. The variances of the magnetization angle and the resistance are calculated using Boltzmann statistics.

Within this description, the expectation value $\langle A\rangle$ of a quantity A at finite temperatures is given by:

$$\langle A\rangle=\frac{1}{Z}\int_0^{2\pi} \mathrm{d}\phi\ \ A(\phi)\exp[-E(\phi)/kT], \tag{3a}$$

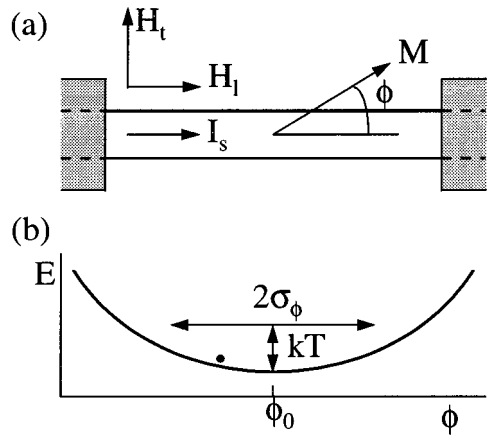

FIG. 8. Schematic overview of (a) the simplified model system and (b) the energy diagram. The magnetization direction ϕ fluctuates around the minimum energy value ϕ_0 due to thermal excitations.

$$Z=\int_0^{2\pi} \mathrm{d}\phi \, \exp[-E(\phi)/kT], \tag{3b}$$

where ϕ is the angle between the magnetization and the longitudinal axis, see Fig. 1. The variance of the quantity A is defined as $\sigma_A^2=\langle A^2\rangle-\langle A\rangle^2$. To lowest order in temperature, the variance σ_ϕ^2 of the magnetization angle around the equilibrium value ϕ_0 (which we assume to be nondegenerate) can be obtained by applying the stationairy phase approximation to Eq. (3), which yields:

$$\sigma_\phi^2=kT\left(\left.\frac{\partial^2 E}{\partial\phi^2}\right|_{\phi=\phi_0}\right)^{-1}. \tag{4}$$

This result is very similar to the expression for the variance in ϕ due to ripple caused by lateral variations in the anisotropy direction, since both effects follow from a similar energy minimalization procedure (see, e.g., Ref. 29 for an overview of ripple theory). The difference is that the latter results in lateral (static) variations of the magnetization direction, which show up in microscopy images[20,25] and in global magnetization measurements,[24] while the former results in variations in the time domain.

For small angle fluctuations, the variance σ_R^2 of the resistance is proportional to the variance σ_ϕ^2 of the magnetization angle:

$$\begin{aligned}\sigma_R^2&=\left(\left.\frac{\partial R}{\partial\phi}\right|_{\phi=\phi_0}\right)^2\times\sigma_\phi^2\\&=kT\left(\left.\frac{\partial R}{\partial\phi}\right|_{\phi=\phi_0}\right)^2\times\left(\left.\frac{\partial^2 E}{\partial\phi^2}\right|_{\phi=\phi_0}\right)^{-1}.\end{aligned} \tag{5}$$

Below, the transfer factor $(\partial R/\partial\phi|_{\phi=\phi_0})^2$ between σ_R^2 and σ_ϕ^2 is abbreviated as η^2.

This result has an intuitive interpretation: the magnetization direction fluctuates in around the energy minimum with a variance inversely proportional to the curvature at the minimum [see Fig. 8(b)]. The curvature at the minimum is a measure for the magnetic stability of the element, a deeper minimum meaning a more stable magnetization direction. The angle fluctuations result in resistance fluctuations via the magnetoresistance effect.

V. APPLICATION TO MODEL SYSTEMS

In this section the results will be presented of calculations for a number of model systems that correspond to the systems investigated experimentally. We model all systems by a single magnetic entity in the form of an infinite stripe of width w and thickness t and a uniform magnetization with an angle ϕ with respect to the long axis of the stripe [see Fig. 8(a)]. The magnetic energy density $E(\phi)$ of each system can be written as the sum of the Zeeman, anisotropy and demagnetization energy densities:

$$\begin{aligned}E(\phi)=&-\mu_0 M_s(H_t\sin\phi+H_l\cos\phi)-K\cos^2\phi\\&-\tfrac{1}{2}\mu_0 M_s H_d\cos^2\phi,\end{aligned} \tag{6}$$

where M_s is the saturation magnetization, K the in-plane (induced) uniaxial anisotropy constant, and $H_{t(l)}$ the applied transverse (longitudinal) magnetic field. The demagnetization field is approximated by $H_d\approx M_s t/w$. Within this model H_d does not depend on the transverse coordinate due to the assumed uniform magnetization direction. The energy terms that occur for GMR-based systems due to interlayer and magnetostatic coupling between the free and pinned layer are neglected. Still assuming a homogeneous magnetization in the free layer, these terms only give rise to a shift along the magnetic field axis.

Without longitudinal field, the magnetization will saturate at the saturation field H_s:

$$H_s=\frac{2K}{\mu_0 M_s}+H_d. \tag{7}$$

By using this field to normalize the applied magnetic field strengths a relatively simple expression is obtained for the normalized energy density $e(\phi)$ (normalized quantities are denoted by lowercase characters):

$$e(\phi)=\frac{E(\phi)}{\mu_0 M_s H_s}=-\tfrac{1}{2}\cos^2\phi-h_t\sin\phi-h_l\cos\phi, \tag{8}$$

where $h_t=H_t/H_s$ and $h_l=H_l/H_s$. The dependencies of the resistance on the angle ϕ have been modelled by:

$$r_{\mathrm{AMR}}(\phi)=\frac{R_{\mathrm{AMR}}(\phi)-R_0}{\Delta R_{\mathrm{AMR}}}=\cos^2\phi, \tag{9a}$$

$$r_{\mathrm{BP}}(\phi)=\frac{R_{\mathrm{BP}}(\phi)-R_0}{\Delta R_{\mathrm{AMR}}}=\cos^2\left(\phi-\frac{\pi}{4}\right), \tag{9b}$$

$$r_{\mathrm{GMR}}(\phi)=\frac{R_{\mathrm{GMR}}(\phi)-R_0}{\Delta R_{\mathrm{GMR}}}=\frac{1}{2}(1-\sin\phi), \tag{9c}$$

in which R_0 is the minimum resistance and ΔR_{AMR} and ΔR_{GMR} are the maximum resistance changes for AMR and GMR, respectively.

Using these expressions, the field dependence of the variance of the resistance is calculated for the three MRE types investigated and a comparison with the experimentally

determined $1/f$ noise level is made. First, the case without longitudinal magnetic field will be described. Later, the dependence on this field will also be discussed, as well as the influence of a small AMR contribution to the noise of a GMR-based MRE.

A. Without longitudinal field

In Fig. 9 the results of the model calculations are pre sented for the three different MRE configurations [only AMR in Figs. 9(a)–9(e), AMR using the barber pole geometry in Figs. 9(f)–9(j) and only GMR in Figs. 9(k)–9(o)] for applied transverse magnetic field only, i.e., $h_l=0$. The top two rows of Fig. 9 represent the variation upon applying a tranverse magnetic field of the equilibrium magnetization direction $\sin\phi_0$ [Figs. 9(a), 9(f), and 9(k)] and the equilibrium resistance $r(\phi_0)$ [Figs. 9(b), 9(g), and 9(l)]. These are calculated from the equilibrium angle ϕ_0 that follows from Eq. (8), and substitution in Eq. (9). The field variations of the variances of the magnetization angle σ_ϕ^2 [third row, Figs. 9(c), 9(h), and 9(m)] and the resistance σ_r^2 [bottom row, Figs. 9(e), 9(j), and 9(o)] are obtained from Eq. (4) and Eq. (5), respectively. The transfer factor $\eta^2=(\partial R/\partial\phi|_{\phi=\phi_0})^2$ between these quantities is shown in the fourth row [Figs. 9(d), 9(i), and 9(n)].

The variation of the magnetization upon appying a transverse magnetic field is the same for all three measuring geometries since all magnetic entities are assumed to be identical. As can be seen in Figs. 9(a), 9(f), and 9(k), for $|h_t|<1$ the transverse magnetization component $M_s\sin\phi_0$ increases linearly with transverse applied field. This is the well known hard-axis magnetization curve for magnetic systems in which the (effective) uniaxial anisotropy is dominant. For $|h_t|\geqslant 1$ the magnetization direction is along the field direction.

The magnetization direction is relatively stable at small applied fields and again in high applied fields, as may be seen from the variance σ_ϕ^2 of the magnetization angle [Figs. 9(c), 9(h), and 9(m)]. At the saturation field ($|h_t|=1$), however, σ_ϕ^2 diverges, a characteristic result which is also present in Hoffmann's linear ripple theory[29] and is qualitatively confirmed by microscopy[20,25] and magnetization[24] data.

The field dependence of the resistance noise for the AMR-based MRE may be understood from Figs. 9(a)–9(e). The resistance change [Fig. 9(b)] upon applying a transverse magnetic field shows the characteristic parabolic behavior for $|h_t|<1$ and saturates to the low resistance state at higher fields. The variance σ_ϕ^2 of the magnetization angle [Fig. 9(c)] diverges as the saturation field is approached, but this is compensated by a vanishing transfer factor η^2 [Fig. 9(d)]. The result is a finite variance σ_r^2 of the resistance at $|h_t|=1$ [Fig. 9(e)]. For $|h_t|<1$ the variance of the resistance increases quadratically with the field, i.e., $\sigma_r^2/kT=4h_t^2$. For higher fields σ_r^2 is zero.

The results for the AMR-based MRE with the barber pole geometry are presented in the Figs. 9(f)–9(j). For this MRE, the divergence of the variance σ_ϕ^2 of the magnetization angle [Fig. 9(h)] is not compensated by a vanishing transfer factor η^2 [Fig. 9(i)] at $|h_t|=1$, and therefore the variance σ_r^2 of the resistance [Fig. 9(j)] diverges, too. The low field part ($|h_t|\ll 1$) may be approximated by $\sigma_r^2/kT\approx(h_t-1)(h_t+1)$. The transfer factor η^2 [Fig. 9(i)] is nonzero above saturation ($|h_t|>1$), and therefore this MRE does have a nonzero variance of the resistance $\sigma_r^2/kT=(|h_t|-1)^{-1}$ in the saturated state, unlike the other two MREs.

Figures 9(k)–9(o) show the results of the model calculations for the GMR-based MRE. For these calculations, it is assumed that only the free layer is able to fluctuate, i.e., the pinned layer is held fixed rigidly with the magnetic moment aligned along the positive h_t direction or, i.e., the pinning to the antiferromagnet is assumed to be sufficiently strong. As discussed above, no magnetic interactions have been assumed between both magnetic layers. For this MRE type, the transfer factor η^2 [Fig. 9(n)] compensates the divergence at $|h_t|=1$ of the variation σ_ϕ^2 of the magnetization angle [Fig. 9(m)]. Like for the AMR-based MRE, this leads to a finite variance σ_r^2 of the resistance at $|h_t|=1$ [Fig. 9(o)]. Within this model, the variance of the resistance $\sigma_r^2/kT=\frac{1}{4}$ for $|h_t|<1$. Because the transfer factor vanishes above saturation also σ_r^2 disappears for $|h_t|>1$.

Both AMR-based MREs show a qualitative similarity between field dependence of the calculated variance of the resistance and the experimentally observed 1/f noise level at 1 Hz. The AMR-based MRE without barber pole indeed shows the double peak structure [Fig. 5(b)], where (as discussed in Sec. III) the difference in the two observed peak heights may be explained by a misalignment of the applied magnetic field. The width of the peaks may be explained by demagnetization or ripple effects. Also for the AMR-based MRE with barber pole the theory reproduces the three experimentally observed peaks [Fig. 6(b)], two large peaks at the saturation fields and a smaller peak at zero field. For the GMR-based MRE the agreement between experiment and theory is less satisfactory. The experiment shows a huge peak [Fig. 7(b)] where the calculations predict a plateau. It will be shown below that by taking a small superimposed AMR effect into account theory will yield a better prediction.

It is noted that within the present model the field dependence of the noise contributions due to thermal excitations and due to field fluctuations are identical for fields $|h_t|\leqslant 1$, if the amplitude of the field fluctuations is independent of the applied field, if no longitudinal magnetic field is applied, and if only a $\cos^2\phi$ anisotropy term is present. When $h_l\neq 0$ or when the anisotropy also contains other terms, both contributions show a different dependence on the applied transverse magnetic field.

B. With longitudinal field

In certain applications a longitudinal field is applied to an MRE, e.g., when domain wall formation should be prevented or when a specific rotation direction is desired. In some cases the longitudinal field is not applied externally, but is already present due to geometrical effects. For example, the current distribution in the metallization layer of the barber pole geometry will generate a field with a longitudinal component.

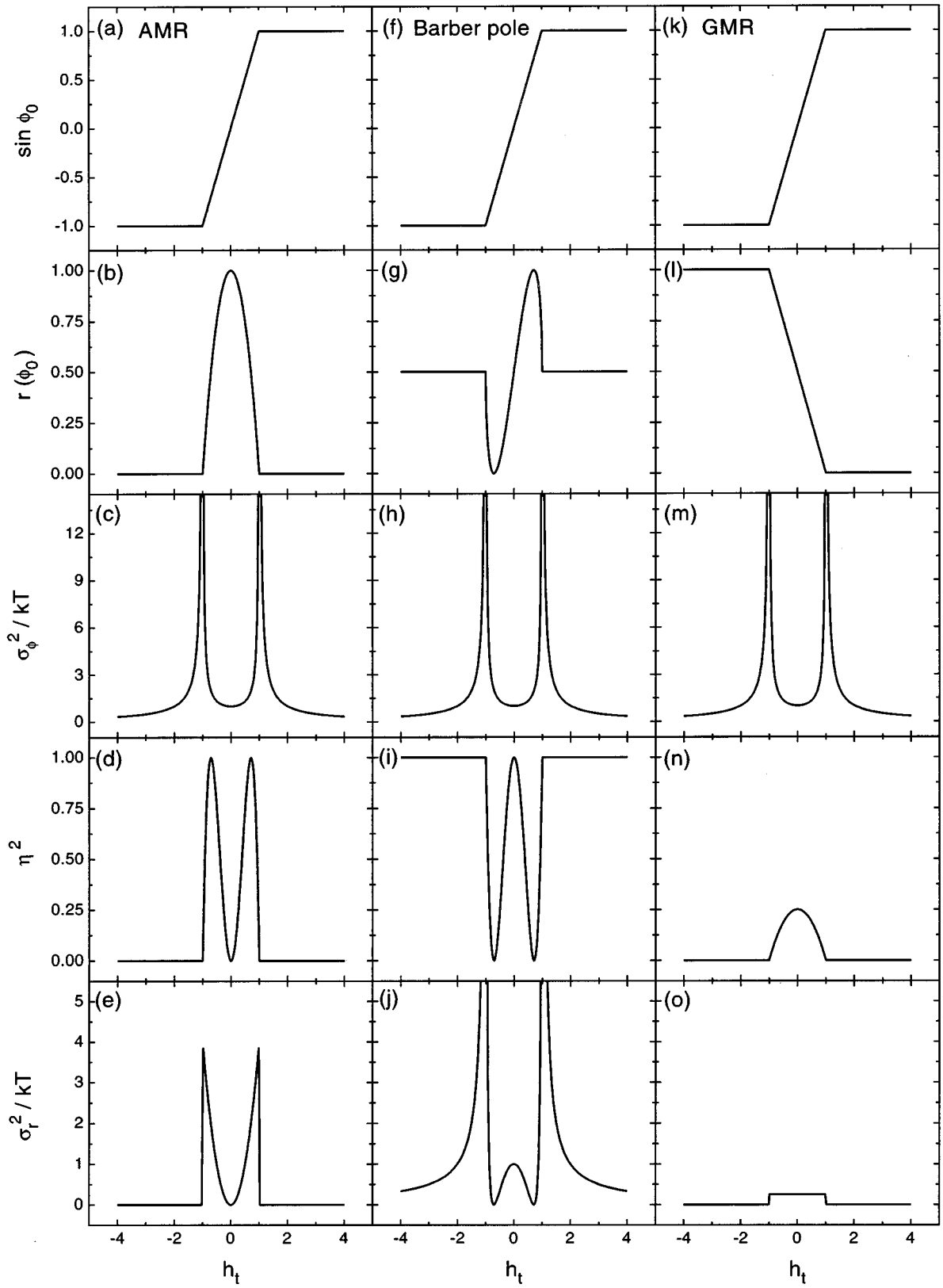

FIG. 9. Results of the model calculations for MREs based on (a)–(e) the AMR effect, (f)–(j) the AMR effect linearized using the barber pole geometry, and (k)–(o) the GMR effect. Only a transverse magnetic field is applied (i.e., $h_l=0$).

The application of a longitudinal field can also be used as a tool to obtain additional insight in the origin of the excess $1/f$ noise. The noise level depends on the magnetic state of the system, which can be changed by the application of a longitudinal field. This can be used as an additional test for the model presented above. In Fig. 10 the calculated effect of a longitudinal field on the magnetic properties of a single magnetic layer is shown. The magnetic response [Fig.

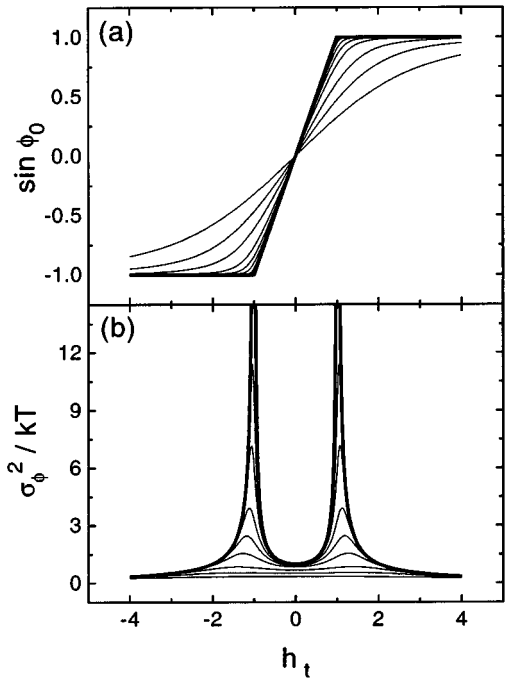

FIG. 10. The calculated effect of a longitudinal magnetic field on (a) the magnetic response and (b) the variance of the magnetization angle of a single magnetic film in an applied transverse field. The different curves are for $h_l=0$ (thick) and $h_l=0.01$, 0.02, 0.05, 0.1, 0.2, 0.5, 1, and 2 (thin), increasing h_l values correspond to (a) a decreasing slope of the sin ϕ_0 curve and (b) a decreasing σ_ϕ^2.

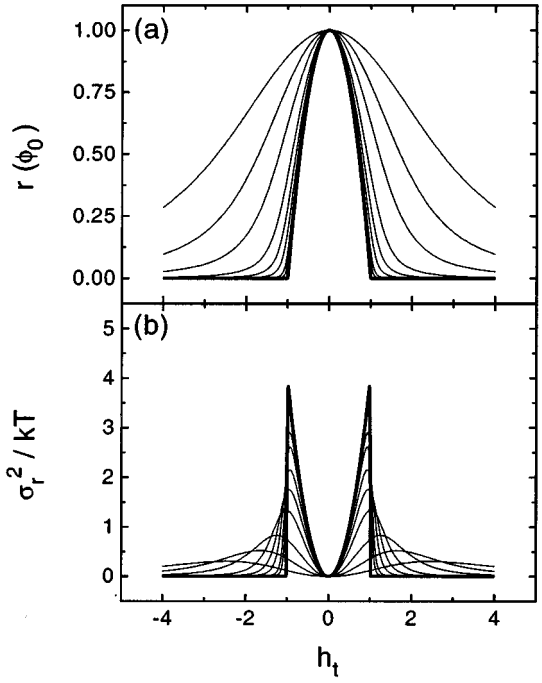

FIG. 11. The calculated effect of an applied longitudinal magnetic field on (a) the MR curve and (b) the variance of the resistance due to thermal excitations of the magnetization direction, for an AMR-based MRE. The different curves are for $h_l=0$ (thick) and $h_l=0.01$, 0.02, 0.05, 0.1, 0.2, 0.5, 1, and 2 (thin), increasing h_l values corresponding to (a) a broadening of the MR curve and (b) a decreasing σ_r^2 at $|h_t|=1$.

10(a)] is smeared out, reflecting the smoother reversal of the magnetic moment upon applying a transverse magnetic field. As a result the variance σ_ϕ^2 of the magnetization angle [Fig. 10(b)] reduces in amplitude in the whole field range and the divergences at $|h_t|=1$ disappear.

A similar broadening is observed in the calculated magnetoresistance curve of an AMR-based MRE, as shown in Fig. 11(a) for increasing applied longitudinal magnetic fields. This means that the MRE sensitivity (slope of the magnetoresistance curve) decreases. As can be seen in Fig. 11(b), also the variance σ_r^2 of the resistance decreases, especially around $|h_t|=1$. Another observation is the shift of the maximum in σ_r^2 to higher transverse fields for increasing longitudinal fields.

Qualitatively, these trends are also observed in the experiment as shown in Fig. 12. The resistance curve [Fig. 12(a)] becomes broader as the longitudinal field is increased and S_V at 1 Hz decreases significantly [Fig. 12(b)]. The shift in the peak position is not resolved experimentally.

The same trends are predicted for the AMR-based MRE with barber pole metallization, as is shown in Fig. 13. The resistance curve broadens [Fig. 13(a)], the maximal variance of the resistance decreases and the field at which the maximum is obtained shifts to higher values [Fig. 13(b)]. Also for the GMR-based MRE a broadening of the resistance [Fig. 14(a)] and the variance of the resistance [Fig. 14(b)] is predicted.

C. Combined GMR and AMR

In the experimental GMR-based MRE, in addition to the GMR effect also an AMR effect is present due to the rotation

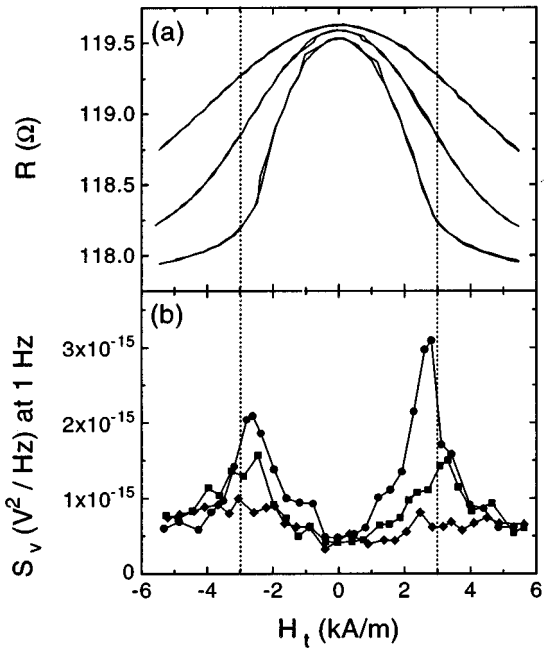

FIG. 12. Experimental observation of the effect of an applied longitudinal magnetic field on (a) the MR curve and (b) the voltage spectral density at 1 Hz for an AMR-based MRE. The applied longitudinal fields are $H_l=0$ (circles), 0.4 (squares), and 1.6 (diamonds) kA/m, corresponding to $h_l=0$, 0.13, and 0.51, respectively. The dashed lines indicate the estimated saturation fields $\pm H_s$ for this geometry.

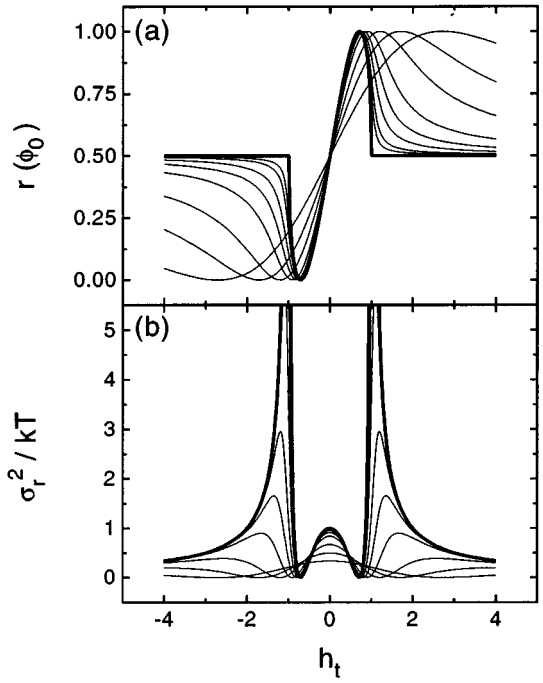

FIG. 13. The calculated effect of an applied longitudinal magnetic field on (a) the MR curve and (b) the variance of the resistance due to thermal excitations of the magnetization direction, for an AMR-based MRE with barber pole metallization. The different curves are for $h_l=0$ (thick) and $h_l=0.01$, 0.02, 0.05, 0.1, 0.2, 0.5, 1, and 2 (thin), increasing h_l values corresponding to (a) a broadening of the MR curve and (b) a decreasing σ_r^2 at $h_t=0$.

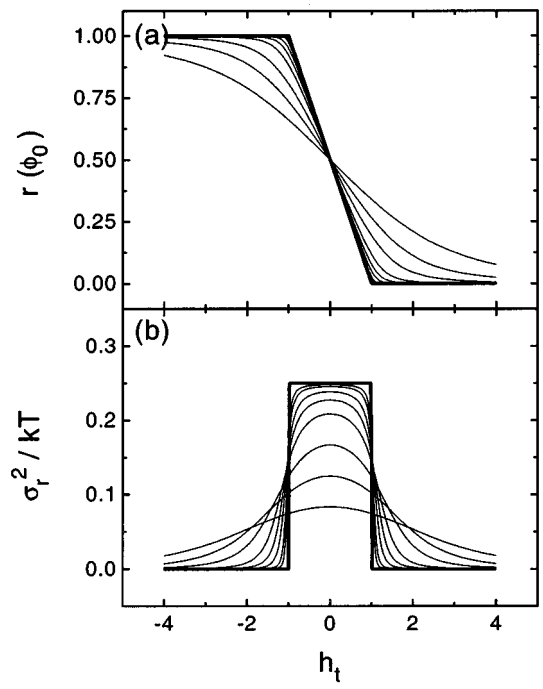

FIG. 14. The calculated effect of an applied longitudinal magnetic field on (a) the MR curve and (b) the variance of the resistance due to thermal excitations of the magnetization direction, for a GMR-based MRE. The different curves are for $h_l=0$ (thick) and $h_l=0.01$, 0.02, 0.05, 0.1, 0.2, 0.5, 1, and 2 (thin), increasing h_l values corresponding to (a) a broadening of the MR curve and (b) a decreasing σ_r^2 at $|h_t|\leqslant 1$.

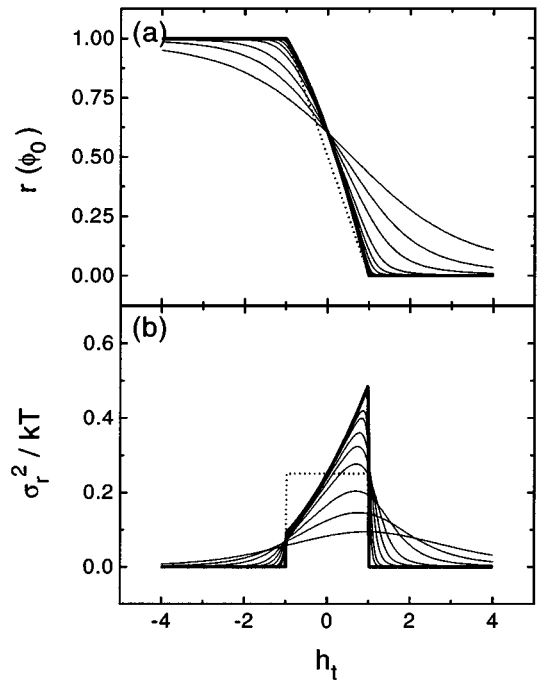

FIG. 15. The calculated effect of an applied longitudinal magnetic field on (a) the MR curve and (b) the variance of the resistance due to thermal excitations of the magnetization direction, for an MRE in which both GMR and AMR are present ($\delta=0.1$). The different curves are for $h_l=0$ (thick) and $h_l=0.01$, 0.02, 0.05, 0.1, 0.2, 0.5, 1, and 2 (thin), increasing h_l values corresponding to (a) a broadening of the MR curve and (b) a decreasing σ_r^2 at $|h_t|\leqslant 1$. The dashed lines are the results for only GMR (i.e., $\delta=0$) without applied longitudinal field (i.e., $h_l=0$).

of the free magnetic layer. This AMR effect, although small compared to the GMR effect, will also have an influence on the noise. Therefore, model calculations have been performed in which both the GMR and the AMR effect are present. The resistance is modelled by:

$$r_{\mathrm{AMR+GMR}}(\phi)=\tfrac{1}{2}(1-\sin\,\phi)+\delta\,\cos^2\,\phi, \tag{10}$$

where δ now represents the amplitude of the AMR effect relative to the GMR effect. Using this formula, the resistance and noise have been plotted in Fig. 15 for $\delta=0.1$. Figure 15(a) shows that as a result of the additional AMR effect the magnetoresistance curve is non-linear. The field dependence of the variance of the resistance due to thermal excitations of the magnetization as shown in Fig. 15(b) is found to be not simply the addition of the contributions due to GMR and AMR. The values at $h_t=\pm 1$ are found to be strongly different and the variance of the resistance (as well as the sensitivity) is expected to be lower than for a pure GMR-based MRE for $h_t<0$. The field dependence of the variance of the resistance can be looked upon as an asymmetric single peak, with a maximum at, or somewhat below $h_t=1$ for small applied longitudinal fields, decreasing gradually down to the negative saturation field. This asymmetric field dependence is roughly as observed in the experiment [Fig. 7(b)]. It should be noted that the amount of asymmetry of the noise is very sensitive to the ratio between the GMR and AMR effect.

VI. DISCUSSION AND CONCLUSIONS

In this article we have presented results of resistance noise measurements on microfabricated magnetoresistive elements based on either the AMR or the GMR effect. These MREs are designed to behave as a single magnetic domain, i.e., domain walls are excluded from the active area of the element. The resistance noise spectra are obtained for frequencies between 10 Hz and 100 kHz under dc sensor operation at room temperature. Thermal resistance noise was the dominant noise source above about 10 kHz. At low frequencies the resistance noise is found to be dominated by a magnetic field dependent $1/f$ contribution. The $1/f$ noise is low in high applied magnetic fields and increases by a factor of ~ 6 (AMR-based elements) to $\sim$ 40 (GMR-based elements) in the most sensitive region of the magnetoresistance curve. The low value is comparable to the $1/f$ noise level which is also found for nonmagnetic metals. The difference between the relative increase in noise level between the AMR- and GMR-based elements can be understood from the larger magnetoresistance effect, the reduced thickness of the layers, and the lower saturation fields for the GMR-based MRE.

The field dependence of the excess $1/f$ contribution could be qualitatively understood from a simple Stoner–Wohlfahrt type model. The model calculates to lowest order in T the variance of the resistance of a thermally excited magnetic moment. The fluctuations of the magnetic moment direction result in resistance fluctuations via the magnetoresistance effect.

The agreement between the model calculations and the experiment is satisfactory for the investigated AMR-based MREs, while for the GMR-based MREs only a rough agreement could be obtained. More detailed measurements of the dependence of the resistance noise on both the applied longitudinal and transverse magnetic fields are needed to test the model. Future improvements of the model should include effects which have been neglected in this article, such as the influences of demagnetization effects, which cause a nonuniform magnetization profile, local anisotropy variations, which cause ripple, coupling between the two magnetic layers, and the coupling between the pinned magnetic layer and the antiferromagnetic layer.

ACKNOWLEDGMENTS

The authors wish to thank J. W. van Est, J. Briaire, L. K. J. Vandamme, D. J. Adelerhof, M. J. M. de Jong, and H. van Houten for fruitful discussions. This work was supported in part by the European Community ESPRIT Long Term Research Project No. 20 027, ''Novel Magnetic Nanodevices of artificially layered Materials $(NM)^2$.''

[1] T. R. McGuire and R. I. Potter, IEEE Trans. Magn. **MAG-11**, 1018 (1975).
[2] M. N. Baibich, J. M. Broto, A. Fert, F. Nguyen Van Dau, F. Petroff, P. Etienne, G. Cruezet, A. Friederich, and J. Chazelas, Phys. Rev. Lett. **61**, 2472 (1988).
[3] G. Binasch, P. Grünberg, F. Saurenbach, and W. Zinn, Phys. Rev. B **39**, 4828 (1989).
[4] B. Dieny, V. S. Speriosu, S. S. P. Parkin, B. A. Gurney, D. R. Wilhoit, and D. Mauri, Phys. Rev. B **43**, 1297 (1991).
[5] T. G. S. M. Rijks, W. J. M. de Jonge, W. Folkerts, J. C. S. Kools, and R. Coehoorn, Appl. Phys. Lett. **65**, 916 (1994).
[6] P. Ripka, Sens. Actuators A **41–42**, 394 (1994).
[7] C. Tsang, J. Appl. Phys. **55**, 2226 (1984).
[8] K. E. Kuijk, W. J. van Gestel, and F. W. Gorter, IEEE Trans. Magn. **MAG-11**, 1215 (1975).
[9] F. N. Hooge, T. G. M. Kleinpenning, and L. K. J. Vandamme, Rep. Prog. Phys. **44**, 31 (1981).
[10] P. Dutta and P. M. Horn, Rev. Mod. Phys. **53**, 497 (1981).
[11] M. B. Weissman, Rev. Mod. Phys. **60**, 537 (1988).
[12] H. T. Hardner, M. B. Weissman, M. B. Salomon, and S. S. P. Parkin, Phys. Rev. B **48**, 16 156 (1993).
[13] H. T. Hardner, S. S. P. Parkin, M. B. Weissman, M. B. Salomon, and E. Kita, J. Appl. Phys. **75**, 6531 (1994).
[14] H. T. Hardner, M. B. Weissman, and S. S. P. Parkin, Appl. Phys. Lett. **67**, 1938 (1995).
[15] H. T. Hardner, M. B. Weissman, B. Miller, R. Loloee, and S. S. P. Parkin, J. Appl. Phys. **79**, 7751 (1996).
[16] L. S. Kirschenbaum, C. T. Rogers, S. E. Russek, and S. C. Sanders, IEEE Trans. Magn. **31**, 3943 (1995).
[17] M. A. M. Gijs, J. B. Giesbers, J. W. van Est, J. Briare, L. K. J. Vandamme, and P. Beliën, J. Appl. Phys. **80**, 2539 (1996).
[18] M. A. M. Gijs, J. B. Giesbers, P. Beliën, J. W. van Est, and L. K. J. Vandamme, J. Magn. Magn. Mater. **165**, 360 (1997).
[19] J. C. S. Kools, J. J. M. Ruigrok, L. Postma, M. C. de Nooijer, and W. Folkerts, IEEE Trans. Magn. (to be published).
[20] J. McCord, A. Hubert, J. C. S. Kools, and M. C. de Nooijer, IEEE Trans. Magn. **32**, 4803 (1996).
[21] F. N. Hooge, Phys. Lett. **29A**, 139 (1969).
[22] K. Fuchs, Proc. Cambridge Philos. Soc. **34**, 100 (1938).
[23] E. H. Sondheimer, Adv. Phys. **1**, 1 (1952).
[24] T. G. S. M. Rijks, R. F. O. Reneerkens, R. Coehoorn, and W. J. M. de Jonge (unpublished).
[25] M. F. Gillies, J. N. Chapman, and J. C. S. Kools, J. Appl. Phys. **78**, 5554 (1995).
[26] R. V. Chamberlain, J. Appl. Phys. **76**, 6401 (1994).
[27] R. V. Chamberlain and M. R. Scheinfein, Science **260**, 1098 (1993).
[28] T. G. S. M. Rijks, R. Coehoorn, J. T. F. Daemen, and W. J. M. de Jonge, J. Appl. Phys. **76**, 1092 (1994).
[29] H. Hoffmann, IEEE Trans. Magn. **MAG-4**, 32 (1968).